RESEARCH ARTICLE

Ne2 encodes protein(s) and the altered RuBisCO could be the proteomics leader of hybrid necrosis in wheat (*Triticum aestivum* L.)

SI RUI PAN[1], XING LAI PAN[2]*, QIAN YING PAN[3], YIN HONG SHI[2], LI ZHANG[2], YUN FAN[2] and YAN RUI XUE[2]

[1] *Life Science and Technology A1201, Beijing University of Chemical Technology, Beijing 102200, People's Republic of China*
[2] *Department of Food Crop Science, Cotton Research Institute, Shanxi Agriculture Science Academy, Yuncheng, Shanxi 044000, People's Republic of China*
[3] *Foreign Language College, Anhui University of Technology and Science, Wuhu, Anhui 241000, People's Republic of China*

Abstract

Wheat hybrid necrosis is caused by the interaction of two dominant complementary genes, *Ne1* and *Ne2*, located on chromosome arms 5BL and 2BS, respectively. The sequences of *Ne1* or *Ne2* have not yet been identified. It is also not known whether *Ne1* and *Ne2* are structural or regulatory genes. Understanding the proteomic pathways may provide a knowledge base for protecting or maximizing the photosynthesis capacity of wheat. Using DIGE and MALDI-TOF-TOF MS, the flag leaf protein patterns of the two unique F_{14} near-isogenic line siblings (NILs), the necrotic ShunMai 12Ah (*Ne1Ne1Ne2Ne2*) and the normal ShunMai 12Af (*Ne1Ne1ne2ne2*) were compared. Due to the presence or absence of *Ne2*, (i) three protein spots were expressed or disappeared, (ii) seven RuBisCO-related proteins were altered significantly, and (iii) 21 photosynthesis/glucose related proteins were changed significantly. Three hypotheses were deduced, (i) *Ne1* may also encode protein(s), (ii) genetic maladjustment of RuBisCO could lead to early leaf death, and (iii) interactions between nuclear genes and chloroplast genes could determine photosynthetic traits. Our hypothetical model presents the RuBisCO pathway of hybrid necrosis in wheat and explains how *Ne1* and *Ne2* interact at molecular level.

[Pan S. R., Pan X. L., Pan Q. Y., Shi Y. H., Zhang L., Fan Y. and Xue Y. R. 2017 *Ne2* encodes protein(s) and the altered RuBisCO could be the proteomics leader of hybrid necrosis in wheat (*Triticum aestivum* L.). *J. Genet*. **96**, 261–271]

Introduction

The world is facing the challenge of producing more wheat on less land and using less water with fewer chemicals (http://www.rothamsted.ac.uk/). Genetic enhancement of the net photosynthetic productivity of wheat represents the most cost-effective and environment-friendly method for increasing sustainable global food security. The 20:20 wheat® focusses on photosynthetic productivity trying to increase wheat yield potential to 20 t/ha within the next 20 years (http://www.rothamsted.ac.uk/).

Wheat hybrid necrosis is literally a genetic early leaf death (GELD) that dramatically reduces photosynthetic longevity and productivity. Progressive lethal or semi-lethal necrosis of F_1 plants in some wheat hybrids is brought about by the two dominant complementary genes (Kostyuchenko 1936; Caldwell and Compton 1943), *Ne1* and *Ne2* (Hermsen 1963a, b), located on chromosome arms 5BL and 2BS, respectively (Chu *et al.* 2006). While *Ne1* and *Ne2* have been reported and characterized, their sequences have not been cloned (Chu *et al.* 2006) and their primary products are yet to be identified. It is also not clear whether *Ne1* and *Ne2* are structural or regulatory genes (Pan *et al.* 2009). When either *Ne1* or *Ne2* is present alone in a wheat genotype (e.g. *Ne1Ne1ne2ne2* or *ne1ne1Ne2Ne2*), the plant is normal. But when found together, hybrid necrosis occurs. How does the two non-harmful genes trigger GELD, has remained unknown. The

*For correspondence. E-mail: pxlwbig@126.com.

Keywords. autoimmune; chlorenchyma; hypersensitive response; posttranslational behaviour; *rbcS*; *rbcL*.

molecular causation of wheat hybrid necrosis has long been a major puzzle since 1929 (Naskidashvili *et al.* 2010). Understanding the proteomics pathway of the GELD is expected to enrich our knowledge base at a molecular level for protecting or even maximizing the photosynthetic longevity and productivity of wheat. The purpose of this study was to ascertain whether *Ne2* encodes protein(s) by using DIGE and MALDI-TOF-TOF MS.

Materials and methods

The two near-isogenic line siblings (NILs) of Ne2: ShunMai 12Ah and ShunMai 12Af

The logical way to understand the proteomic behaviour of a gene is to observe the effects of silencing that gene, i.e. to shut off or knock out the gene, and then to see what happens. As the sequences of *Ne1* and *Ne2* are not known yet, the molecular gene-silencing techniques could not be used to shut off *Ne1* or *Ne2*. The development of NILs with different compositions of *Ne* genes is crucial for further identification of their encoded products and molecular functions. Therefore, we spent about 20 years to create the two F_{14} NILs: the necrotic ShunMai 12Ah of the homozygous dominant genotype *Ne1Ne1Ne2Ne2*, vs the normal ShunMai 12Af of the *Ne1Ne1ne2ne2* genotype (Pan *et al.* 2015a). Theoretically, in the F_{14} population, the necrotic ShunMai 12Ah and the normal ShunMai 12Af have 99.99% genetic similarity. Their most distinct phenotypic difference in the growing season is that each leaf (from the very first leaf to the last flag leaf) of the necrotic ShunMai 12Ah died in 18–22 days, while each leaf of the normal ShunMai 12Af remained green for 52–56 days (Pan *et al.* 2015a). These contrasting materials are crucial for ascertaining whether *Ne2* encodes protein(s) or not.

Leaf sampling

The representative plants at the sampling day are shown in figure 1. When the flag leaves of the necrotic ShunMai 12Ah (figure 1a) had fully extended and were totally green while the other stem–leaves were completely dead, the top halves (figure 1c) of the six totally green flag leaf blades were rinsed with distilled water, then cut/wrapped/labelled as one replicate and placed immediately in liquid nitrogen. Three replicates from the necrotic ShunMai 12Ah and three replicates from the normal ShunMai 12Af (figure 1b), were sampled and labelled as 12Ah1X, 12Ah2X, 12Ah3X, 12Af1X, 12Af2X and 12Af3X, respectively.

Protein preparation

Each sample was ground into fine powder in liquid nitrogen from which ~1 g was transferred into a tube containing 25 mL of trichloroacetic acid / acetone (1:9, v/v) as well as 65 mM DDT, and the protein was then precipitated

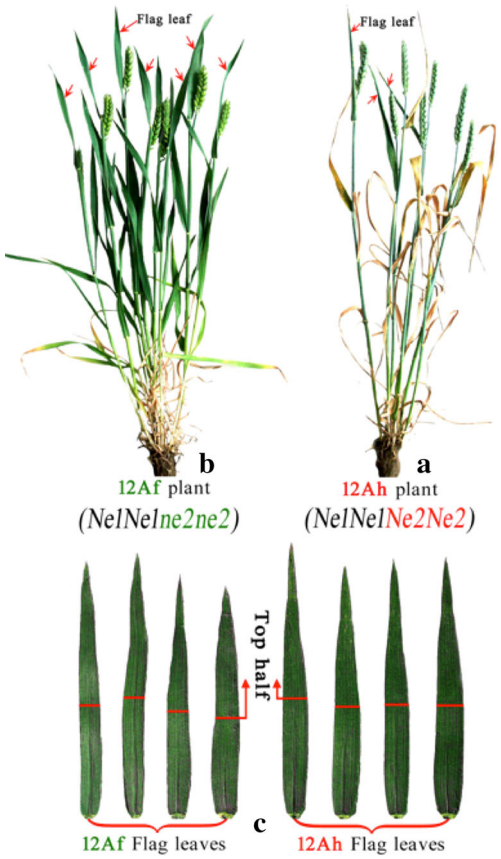

Figure 1. Comparisons of the sampled plants and flag leaves. (a) One representative plant of the necrotic ShunMai 12Ah on the sampling day; the flag leaves of some stems were still totally green, the other stem–leaves of each stem were all totally necrotic due to the *Ne1Ne1Ne2Ne2* genotype. (b) One representative plant of the normal ShunMai 12Af on the sampling day; each stem has 3–5 green leaves including the flag leaf due to *Ne1Ne1ne2ne2* genotype that is lacking *Ne2*. Each leaf (from the very first leaf to the last flag leaf) of the necrotic ShunMai 12Ah died in 18–22 days. In contrast, each leaf of the normal ShunMai 12Af remained green for 52–56 days. (c) What the sampled flag leaves looked like on the sampling day. The top half of each fully green flag leaf was sampled for protein analysis.

at −20°C for 1 h. The sample tubes were centrifuged at 10,000 rpm for 45 min and the supernatants were discarded. Twenty-five mL of acetone was added to each precipitate and the tube was stored at −20°C for 1 h and centrifuged again at 10,000 rpm at 4°C for 45 min. The precipitate was then vacuum dried, weighed and stored at −80°C. A total of 200 mg of protein sample was added to 0.5 mL of DIGE lysis buffer containing 7 M urea, 2 M thiourea, 4% (w/v) CHAPS and 0.2% (v/v) immobilized pH gradient (IPG) buffer. The protein concentration in the supernatant was quantified by the Bradford method using Bio-Rad protein assay reagent. Aliquots of the protein samples were stored at −80°C until use in proteomic analysis.

Table 1. Experimental design for protein labelling.

	Gel1	Gel2	Gel3
Cy2	IS	IS	IS
Cy3	12Ah1X	12Af2X	12Ah3X
Cy5	12Af3X	12Ah2X	12Af1X

IS, internal standard.

Protein labelling using DIGE dyes

The protein samples were labelled using fluorescent CyDyes^{TM} (Cy2, Cy3, and Cy5) developed for DIGE (GE Healthcare, Little Chalfont, UK). The experimental design using the three-dye approach is illustrated in table 1. Fifty μg of an internal standard (IS) containing an equal amount of the six sample proteins was labelled with 400 pmol Cy2. Fifty μg of each sample was labelled with 400 pmol Cy3 or Cy5. A dye swap between 12Ah and 12Af protein samples was carried out to avoid artifacts due to preferential labelling. Protein samples were maintained on ice and fluorescently labelled in the dark for 30 min. The reaction was then quenched by incubating with 1 μL of 10 mM L-lysine (GE Amersham Biosciences) on ice in the dark for 15 min.

2D-DIGE

For each gel, Cy2-labelled, Cy3-labelled, and Cy5-labelled proteins (50 μg each) were pooled and an equal volume of rehydration buffer (8 M urea, 4% CHAPS, 2% DTT and 2% IPG buffer pH 3–10) was added so that the final concentration of DTT and IPG buffer was 1%. The pooled protein samples were subjected to isoelectric focussing (IEF) carried out by the Ettan IPGphor IEF system (GE Amersham) and the nonlinear IPG strips (pH 3–10, 13 cm, GE Healthcare). The IPG strips were rehydrated for 12 h in 250 μL of rehydration buffer containing the protein samples. IEF was performed in four steps: 30 V for 12 h, 500 V for 1 h, 1000 V for 1 h, and 8000 V for 8 h. After the IEF run was completed, the gel strips were equilibrated under gentle shaking for 15 min in equilibration buffer (50 mM Tris-HCl (pH 8.8), 6 M urea, 2% SDS, 30% glycerol, and 1% DTT). This step was repeated using the same buffer with 4% iodoacetamide in place of 1% DTT. The strips were then subjected to the second-dimensional electrophoresis after transfer onto 12.5% SDS-polyacrylamide gels. The second-dimension gels were cast between low fluorescent Pyrex glass plates (16 cm × 14 cm × 1 mm, GE Healthcare) to minimize background fluorescence during scanning. Electrophoresis was performed using the Hofer SE 600 system (GE Amersham) at 15 mA per gel for 30 min, followed by 30 mA per gel until the bromophenol blue reached the end of the gel.

Image acquisitions, analysis and processing

The gels were scanned using a Typhoon FLA 9000 Biomolecular Imager (GE Healthcare). Excitation and emission wavelengths for Cy2, Cy3, and Cy5 were 488/520, 532/580 and 633/670 nm, respectively. Gels were scanned at 100 μm resolution and the photo multiplier tube voltage was set to values ranging between 500 and 700 V to ensure maximum pixel intensity of 50,000 and 80,000 pixels for the three dyes.

Spot identification, background elimination, point matching and differential analysis of the protein spots were all completed using 2D differential in-gel analysis and biological variance analysis (DeCyder) software module; GE. The biological variation analysis module was used for integral matching of the internal standard and all the gel samples were subjected to comparative cross-gel statistical analysis based on spot volumes with a *t* test. P value <0.05 was considered statistically significant.

2D gel excision, tryptic digestion

Protein extracts were separated on preparative gels and proteins of interest were recovered from the gels for identification. Proteins (400 μg) from 12Af1X and 12Ah2X were resolved on separate preparative polyacrylamide gels and were visualized by staining with a modified silver staining methods compatible with subsequent mass spectrometric analysis. All the differentially expressed spots (>1.5-fold) were selected and excised manually from the two preparative gels. Each protein spot of interest cut from the preparative gels was destained for 20 min in 30 mM potassium ferricyanide/100 mM sodium thiosulphate (1:1 v/v) and washed with Milli-Q water until the gel pieces were destained, then was incubated in 0.2 M NH_4HCO_3 for 20 min and then lyophilized. Each spot was digested overnight in 5 ng μL^{-1} trypsin in 25 mM NH_4HCO_3. The peptides were extracted thrice with 60% ACN/0.1% TFA. The extracts were pooled and dried completely by a vacuum centrifuge.

MALDI-TOF-TOF MS analysis

MALDI-TOF-TOF instrument (4800 proteomics analyser) parameters were set using the 4000 Series Explorer software (Applied Biosystems, Foster City, USA). The MS spectra were recorded in reflector mode in a mass range from 800 to 4000 with a focus mass of 2000. MS used a CalMix5 standard to calibrate the instrument (ABI 4700 calibration mixture). For one main MS spectrum 25 subspectra with 125 shots per subspectrum were accumulated using a random search pattern. For MS calibration, autolysis peaks of trypsin ([M + H] + 842.5100 and 2211.1046) were used as internal calibrates, and up to 10 of the most intense ion signals were selected as precursors for MS/MS acquisition, excluding the trypsin autolysis peaks and the matrix ion signals. In MS/MS

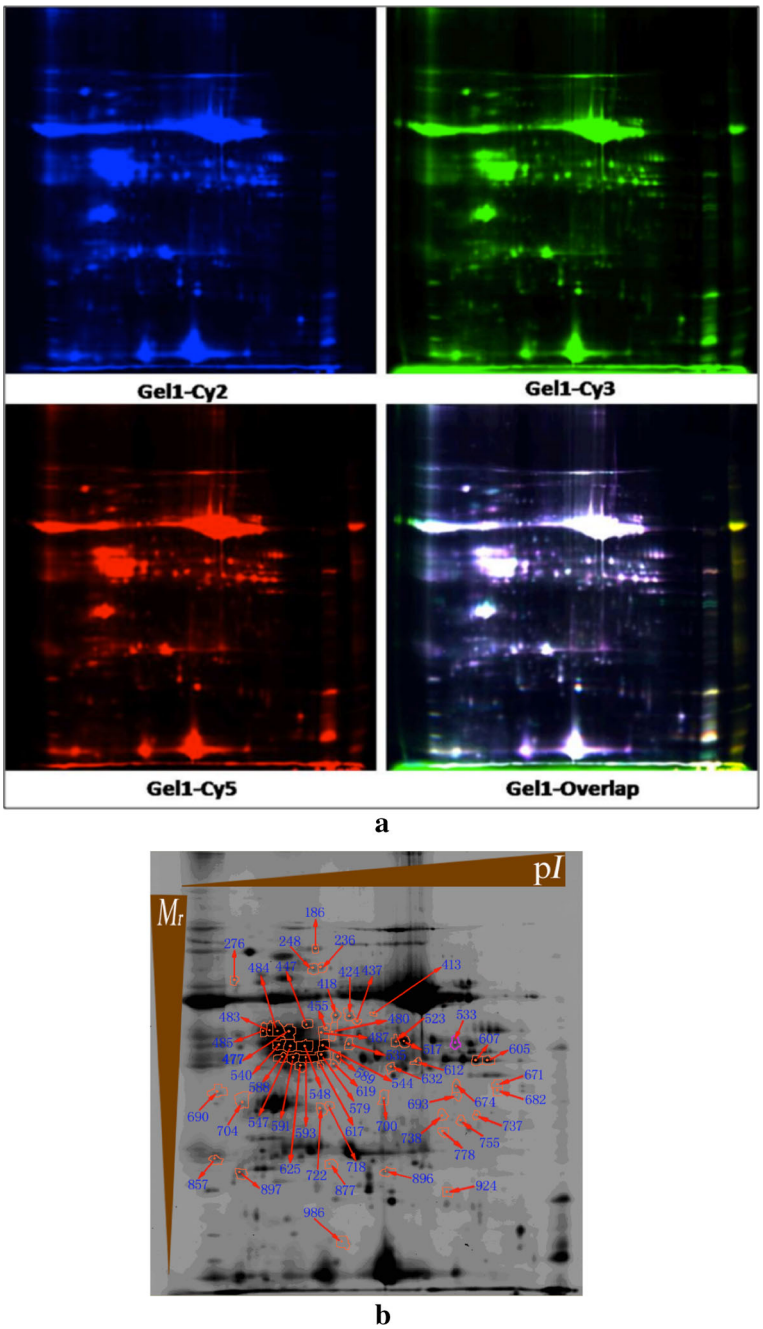

Figure 2. (a) The representative 2D-DIGE image (Gel1). (b) The 31 significantly upregulated protein spots (arrow towards the number) and the 24 significantly downregulated protein spots (arrow towards the spot) in the normal ShunMai 12Af compared to the necrotic ShunMai 12Ah on a representative 2D gel.

positive ion mode, for one main MS spectrum 50 subspectra with 50 shots per subspectrum were accumulated using a random search pattern. The collision energy was 2 kV, the collision gas was air, and the default calibration was set using the Glu1-Fibrinopeptide B ([M + H] + 1570.6696) spotted onto Cal 7 positions of the MALDI target. Combined peptide mass fingerprinting PMF and MS/MS queries were performed by using the MASCOT search engine 2.2 (Matrix Science, Boston, USA) embedded into GPS-explorer software 3.6 (Applied Biosystems) on the NCBI database Viridiplantae with the following parameter settings: 100 ppm mass accuracy, trypsin cleavage one missed cleavage allowed, carbamidomethylation set as fixed modification, oxidation of methionine was allowed as variable modification, MS/MS fragment tolerance was set to 0.4 Da. A GPS explorer protein confidence index ≥95% was used for further manual validation.

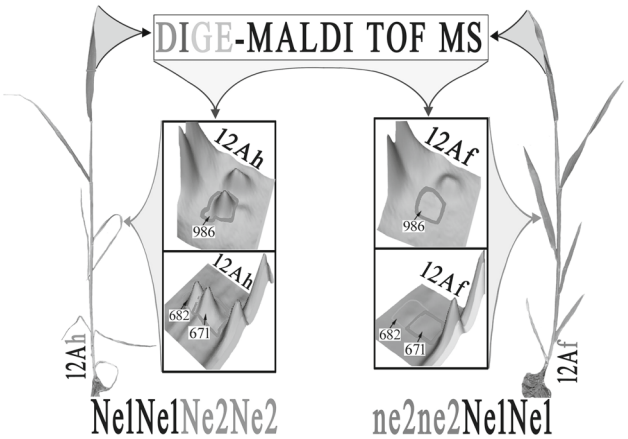

Figure 3. The 3D visualization of the three missing proteins 986, 682 and 671 in the normal ShunMai 12Af compared to the necrotic ShunMai 12Ah.

Results

Fifty-five differentially expressed protein spots

Each 2D gel detected 1267 reproducible protein spots ($n = 9$). DIGE acquisition (figure 2a) and 2D DeCyder software analysis revealed 24 significantly downregulated and 31 upregulated protein spots in the normal ShunMai 12Af compared to the necrotic ShunMai 12Ah (figure 2b).

Three protein spots disappeared due to the absence of Ne2

The three protein spots 986, 682, and 671, which were readily detectable in the necrotic ShunMai 12Ah, were absent in the normal ShunMai 12Af that did not contain *Ne2* (figure 3). This qualitative difference suggests that *Ne2* could encode one or two or three of those proteins (986, 682 and 671) because it was reported (Caldwell and Compton 1943) that the loss of *Ne* genes could be resulted from chromosomal aberration (Pan *et al.* 2015a). It is rational to suppose that protein spots 986, 682 and 671 might be located on the same lost fragment of chromosome 2BS.

The top 10 proteins matched in the database by spot 986 were all large subunits (LSUs) of dicotyledon. Because *Ne2* is a nuclear gene, it could not encode the LSUs. In addition, the gels gave protein 986 the molecular weight of ~15 kD which is of the correct order for the small subunits (SSUs) (12–18 kD) and is much less than that of the LSU (52–55 kD) (Mehta *et al.* 1992). Therefore protein 986 was first deduced to be a heterogeneous SSU of RuBisCO or at least to be involved closely with RuBisCO.

Identifications of the 32 differentially expressed proteins

The top 32 significantly changed proteins were analysed by MALDI-TOF-TOF MS and the database-matched identifications are summarized in table 2. The other 23 changed proteins that were not analysed by MALDI-TOF-TOF MS are listed in table 3.

The 21 photosynthesis/glucose-related proteins

Of the 32 identified proteins, 21 were photosynthesis/glucose-related proteins (of which seven proteins were upregulated and 14 proteins were downregulated significantly in the normal ShunMai 12Af), six were Met/Cys/Adenine-metabolism related proteins, three were disease-resistance related proteins, and two were antioxidant-related proteins (figure 4).

The seven RuBisCO-related proteins

Seven of the 21 photosynthesis/glucose related proteins are involved in RuBisCO. Proteins 480 (RuBisCO activase), 544 (RuBisCO activase) and 700 (SSU precursor), were upregulated, while proteins 612 (RuBisCO activase), 632 (SSU) and 896 (SSU) were downregulated significantly, and in contrast, protein 986 (LSU) was absent in the normal ShunMai 12Af. It is now clear that the subunits of the RuBisCO were altered by proteins 700, 632, 896 and 986, and the activity of RuBisCO activase system were changed by proteins 480, 544, and 612 in the normal ShunMai 12Af that lacked *Ne2*.

There are three unique findings when we sum up all these results: (i) the two NILs, the necrotic ShunMai 12Ah of the homozygous dominant genotype *Ne1Ne1Ne2Ne2* vs the normal ShunMai 12Af of the *Ne1Ne1ne2ne2* genotype; (ii) proteins 986, 682 and 671 were absent in the normal ShunMai 12Af due to the absence of *Ne2*; (iii) the composition and activity of the RuBisCO were evidently altered due to the absence of *Ne2*.

Discussion

Hypothetic RuBisCO maladjustment model

The three unique points mentioned above encouraged us to postulate the following hypothetical RuBisCO maladjustment model. The nuclear gene *Ne2* could encode protein 986 that represents at least one copy of the SSUs. That copy encoded by *Ne2* might be maladjusted to the LSUs encoded by *Ne1*'s *rbcL*. Such maladjustment might increase the oxygenase activity and the production of superoxide species such as H_2O_2 in a cumulative and dynamic way, then affected the other germane proteins changing, finally leading to the early leaf death (figure 5).

Evolutionarily speaking, common wheat is an allohexaploid species (AABBDD) derived from natural hybridizations among at least three diploid ancestor grasses. In the nature of things, common wheat must have at least three types of chloroplast-genomes (A, D and B). Therefore the interactions between different chloroplast *rbcL* genes and different nuclear *rbcS* genes certainly lead to different RuBisCO effects. The bifunctional holoenzyme RuBisCO is composed of eight LSUs encoded by the chloroplast *rbcL* genes and eight SSUs encoded by

Table 2. Identification of the proteins.

	Af/Ah	*P* value (*t*-test)	*Mr*/pI (exp.)	Protein name	Accession no.	*Mr*/pI (cal.)	PC	PSc	PSc C.I. %	Possible function
248	−1.39	0.005	65/5.3	Bp2A protein, partial (*Triticum turgidum* subsp. *dicoccon*)	gi|133872360	25.8/5.86	14	696	100	Glucose catabolic process
236	−1.32	0.014	65/5.5	Bp2A protein, partial (*T. turgidum* subsp. *dicoccon*)	gi|133872360	25.8/5.86	17	779	100	Glucose catabolic process
413	−1.56	0.018	45/6.2	Peroxidase 8 (*T. monococcum*)	gi|57635161	38.1/6.59	8	303	100	Antioxidant
418	−1.48	0.008	45/5.8	S-adenosylmethionine synthase 3; =AdoMet synthase 3;	gi|122220777	43.1/5.51	15	894	100	Methyl donor, S-metabolism, Met/Cys
424	−1.63	0.002	45/6.0	PREDICTED: S-adenosylmethionine synthase 1-like isoform 1 (*Brachypodium distachyon*)	gi|357132007	43.2/5.51	15	806	100	Methyl donor, S-metabolism, Met/Cys
523	−1.3	0.013	38/6.8	Putative PDI-like protein (*T. aestivum*)	gi|299469376	40.6/6.17	11	348	100	Peptide folding process, Met/Cys
533	−1.31	0.006	38/7.7	Glyceraldehyde-3-phosphate dehydrogenase (*T. aestivum*)	gi|253783729	36.6/6.67	14	636	100	Break down glucose; initiation of apoptosis
612	−2.24	0.005	33/7.0	Ribulose-1,5-bisphosphate carboxylase activase (*T. aestivum*)	gi|37783283	22.5/4.98	11	345	100	RuBisCO activase
619	−1.46	0.021	33/5.9	Cysteine synthase; AltName: O-acetylserine sulfhydrylase	gi|585032	34.2/5.48	18	840	100	S-metabolism, Met/Cys
632	−1.4	0.041	32/6.5	Ribulose-1,5-bisphosphate carboxylase/oxygenase small subunit (*T. aestivum*)	gi|4038719	18.8/8.83	7	107	99.99	RuBisCO SSU
671	−5.28	0.001	31/8.3	Pentatricopeptide repeat-containing protein (*Arabidopsis thaliana*)	gi|15228257	74.2/6.8	13	62	22.62	Seedling-specific albino phenotype
674	−1.32	0.004	31/7.7	Vacuolar ATP synthase subunit E (*T. aestivum*)	gi|85375922	26.2/6.38	17	591	100	Calvin cycle, Chloroplast
682	−5.51	0.001	31/8.2	Glucan endo-1,3-beta-D-glucosidase (*T. aestivum*)	gi|3757682	35.4/8.8	6	470	100	Disease resistance, glucose process
690	−3.61	0.001	30/4.1	Beta-1,3-glucanase precursor (*T. aestivum*)	gi|4741850	34.8/4.35	4	175	100	Disease resistance, glucose process
693	−1.77	0.008	30/7.6	Class I chitinase (*T. aestivum*)	gi|38112709	34.4/6.89	4	431	100	Disease resistance

Table 2 (*contd*)

	Af/Ah	*P* value (*t*-test)	*Mr*/pI (exp.)	Protein name	Accession no.	*Mr*/pI (cal.)	PC	PSc	PSc C.I. %	Possible function
704	−1.31	0.002	29/4.6	PREDICTED: oxygen-evolving enhancer protein 1, chloroplastic-like isoform 1 (*Brachypodium distachyon*)	gi|357111487	34.8/5.74	8	103	100	Photosynthesis, Chloroplast
722	−2.18	0.003	29/5.9	Beta-1,3-glucanase precursor (*T. aestivum*)	gi|4741846	34.9/5.69	6	448	100	Disease resistance, glucose process
737	−1.3	0.011	27/7.9	Predicted protein (*Hordeum vulgare* subsp. *vulgare*)	gi|326496737	26.5/7.66	13	660	100	Adenine, Purine metabolism
755	−1.26	0.044	26/7.8	Small Ras-related GTP-binding protein (*T. aestivum*)	gi|16903082	25.5/6.66	17	844	100	Regulates gene expression, disease resistance
877	−1.21	0.023	23/5.8	Predicted protein (*Hordeum vulgare* subsp. *vulgare*)	gi|326509981	29.4/7.71	6	306	100	Chloroplast
896	−1.28	0.022	22/6.7	Putative rubisco small subunit (*T. durum*)	gi|62176930	19.3/8.59	9	275	100	RuBisCO SSU
924	−1.78	0.002	18/7.6	Glutathione peroxidase-like protein (*T. aestivum*)	gi|32400826	13.3/9.08	4	60	0	Antioxidant, S-metabolism, Met/Cys
986	−4.01	0.014	15/6.0	Ribulose-1,5-bisphosphate carboxylase/oxygenase large subunit (*Lobelia leschenaultiana*)	gi|89887755	52.0/6.22	9	143	100	RuBisCO LSU
186	1.45	0.040	68/5.5	PREDICTED: transketolase, chloroplastic-like (*Brachypodium distachyon*)	gi|357110873	80.1/5.93	14	405	100	Calvin cycle
276	1.22	0.015	60/4.2	ATP synthase CF1 alpha subunit (*Hordeum vulgare* subsp. *vulgare*)	gi|118430385	55.3/6.32	9	122	100	Disease relevance
480	1.44	0.026	42/5.8	Ribulose 1,5-bisphosphate carboxylase activase isoform 1 (*Hordeum vulgare* subsp. *vulgare*)	gi|167096	47.3/8.62	15	406	100	RuBisCO activase
544	1.38	0.012	38/5.8	Chloroplast ribulose-1,5-bisphosphate carboxylase activase (*T. aestivum*)	gi|115392208	40.3/6.52	17	614	100	RuBisCo activase
591	1.35	0.0003	35/5.5	Chloroplast fructose-bisphosphate aldolase (*T. aestivum*)	gi|223018643	42.2/5.94	12	597	100	Calvin cycle
605	1.4	0.04	33/8.1	Predicted protein (*Hordeum vulgare* subsp. *vulgare*)	gi|326531332	41.0/8.87	23	1240	100	Chloroplast
617	1.4	0.011	33/5.8	PREDICTED: fructose-bisphosphate aldolase, chloroplastic-like (*Brachypodium distachyon*)	gi|357157399	42.2/6.26	8	153	100	Carbon fixation, Oxygenic photosynthesis, chloroplast
700	1.26	0.012	29/6.7	Ribulose-bisphosphate carboxylase (EC 4.1.1.39) small chain precursor (clone 234)—wheat (fragment)	gi|82619	15.6/8.95	4	129	100	RuBisCO SSU precursor
897	1.41	0.047	22/4.7	Rec name: full=2-Cys peroxiredoxin BAS1, chloroplastic	gi|2499477	23.4/5.48	9	482	100	Antioxidant

SN, spot number; Af/Ah, upregulated in 12Af's; −Af/Ah, downregulated in 12Af's; *Mr*, mass (kDa); pI, isoelectric point; exp., observed; cal., theoretical; PC, protein count; PSc, protein score.

Table 3. The other 23 changed proteins in 12Af that were not analysed by MALDI-TOF-TOF MS.

	Af/Ah	*P* value (*t*-test)
437	1.28	0.015
447	1.27	0.013
455	1.26	0.015
477	1.33	0.018
483	1.27	0.001
484	1.28	0.008
485	1.21	0.033
487	1.27	0.031
517	1.24	0.028
535	1.32	0.020
540	1.30	0.025
547	1.34	0.002
548	1.27	0.044
579	1.34	0.006
588	1.32	0.005
589	1.20	0.007
593	1.32	0.008
607	1.37	0.028
625	1.27	0.003
718	1.35	0.035
738	−1.23	0.014
778	1.20	0.021
857	1.21	0.021

the nuclear *rbcS* genes. That is to say, the production of RuBisCO needs the cooperation or complementation of nuclear genes and chloroplast genes. RuBisCO activity is not always balanced for optimal crop productivity (Mehta *et al.* 1992). The *rbcS* gene family of *Triticum* has more than 10 copies located at different sites on the genome, the wheat RuBisCOs are a collection of heterogeneous holoenzyme composed of different SSUs (Dean and Dunsmuir 1989). The B type cytoplasm demonstrates higher RuBPCase activity than those of D type cytoplasm (Evans and Austin 1986). In fact, a large number of interspecies hybrids featured necrotic leaves in their F_1 plants. For example, one of the interspecies hybrids, the F_1 plants of *T. turgidum durum* (BBAA)/*Aegilops tauschii* (DD) featured necrotic leaves (Kenan-Eichler *et al.* 2011), that might have implied a maladjustment between the AABB's LSUs and the DD's SSUs.

Chloroplast degeneration is the consequence of wheat hybrid necrosis

The microscopic observations confirmed that chloroplast degeneration as a consequence of 'hybrid necrosis' in wheat (Toxlpeus and Hermsen 1964). We also observed that the mesophyll cells of the necrotic ShunMai 12Ah died neatly following the chloroplast → chromoplast → gerontoplast steps (figures 6 and 7). The cell death process confirmed that morphologically chloroplasts died first. These observations also strongly support the hypothetical RuBisCO maladjustment model that leads to the chloroplast-pathway cell death.

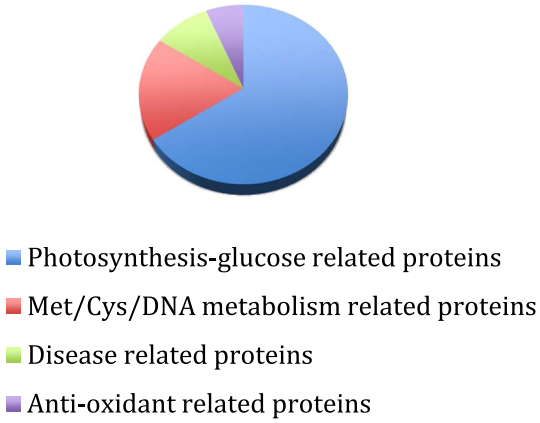

Figure 4. Functional categorization of the identified proteins. Twenty-one are photosynthesis/glucose-related proteins. Six are Met/Cys/Adenine metabolism-related proteins. Three are disease resistance-related proteins. Two are antioxidant-related proteins.

Rethinking the autoimmunity model

Plant hybrid necrosis could result from autoimmunity, perhaps as a pleiotropic effect of the evolution of genes that are involved in pathogen response (Bomblies and Weigel 2007). *Tsn1*–ToxA interactions are associated with wheat necrosis and photosynthesis pathways (Farisa *et al.* 2010). To compare with those two hypothetic models on plant hybrid necrosis, in our study, proteins 276, 693 and 755 were all related to disease resistance; protein 682 was also associated with plant defense responses and closely related to the immune systems. Because protein 682 was also lost in the normal ShunMai 12Af, we may well assume that *Ne2* encoded protein 682, and postulate an autoimmune model. However, we have to consider the following six points carefully. (i) It is known that *Ne2* is tightly linked to *Lr13,* which in turn tightly linked to *Lr23*. Both *Lr13* and *Lr23* confer effective rust fungus resistance (Pukhalskiy *et al.* 2000). Because proteins 682 and 693 are pathogen-related (PR) proteins, they are more likely to be the product of *Lr13* and *Lr23* tightly linked to *Ne2*, rather than the products of *Ne2* itself. (ii) Protein 682 was matched to glucan endo-1,3-beta-D-glucosidase (a polypeptide of 335 AA in wheat), which is responsible for the hydrolysis of beta-glucans, a process that does not produce any superoxide species that should increase dramatically in hybrid necrosis leaves (Khanna-Chopra *et al.* 1998). (iii) An autoimmune process should not occur only in leaves. Glucan endo-1,3-beta-D-glucosidase (protein 682) in wheat is not only in the chlorenchyma but also in root cells. However, the root cells are all normal in the necrotic plants of wheat (Caldwell and Compton 1943). Thus, even if the autoimmune process occurs only in the chlorenchyma, the question

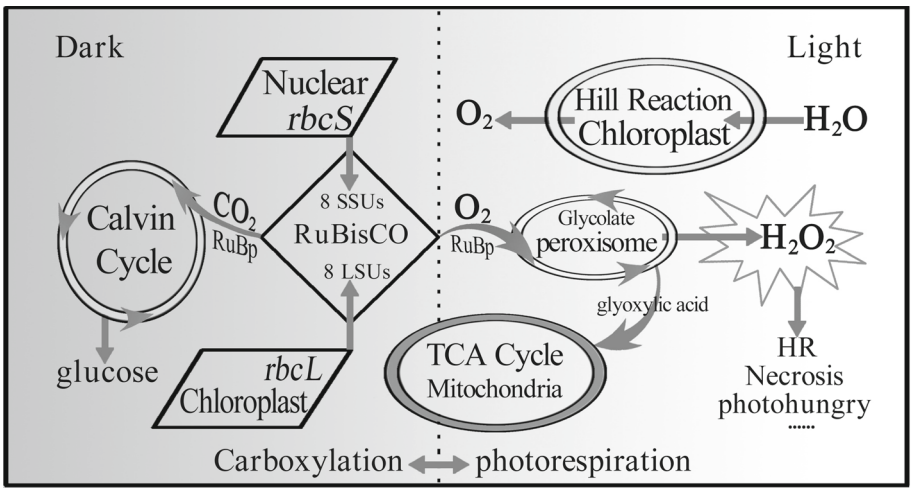

Figure 5. Hypothetical RuBisCO maladjustment model. If any SSU were maladjusted to the LSUs, the balance of carboxylase/oxygenase activity of RuBisCO would be changed. If the photorespiration increased to a certain level, accumulated superoxide species such as H_2O_2 would destroy the chloroplasts directly, which would cause the disastrous conglomeration of mesophyll cell content and lead to the so-called necrosis. H_2O_2 is also used as a potent antimicrobial agent when cells are infected with a pathogen, and that would activate the antioxidant and/or immune systems causing hypersensitive response (HR).

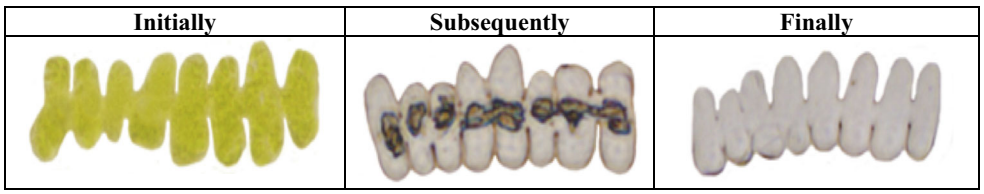

Figure 6. Light microscopic images of the dying mesophyll cells in pinnate-shape. Initially, plasmolysis startes; subsequently, cytoplasm shrinkage/condensation; finally, cytoplasm exhausted empty cells, the cell wall was maintained and unchanged. Vacuoles and condensation of nucleus could not be seen (for method details see Pan *et al.* 2015b).

arises as to why the necrosis always starts at the leaf tip of the oldest leaf and gradually proceeds to the leaf base, rather than starting at all parts of the leaf blade simultaneously. (iv) H_2O_2 is also used as a potent antimicrobial agent when cells are infected by pathogens, which could also lead to the hypersensitive cell death. (v) Glucan endo-1,3-beta-D-glucosidase in wheat cannot change the structure of LSUs or SSUs. The maladjusted RuBisCO can produce and accumulate superoxide species that can also activate resistance responses including glucosidase. (vi) In an autoimmune process, antibodies must occur. However, no new protein spots, i.e. no antibodies were detected in the necrotic F_1s of the parents Pan555 and Zheng891 (Jiang *et al.* 2008; Pan *et al.* 2009). These six arguments make us favour the hypothetical RuBisCO maladjustment model.

To further confirm this model, we urgently need to try: (i) test the other eight NILs hoping to obtain the *Ne1* NILs to confirm if *Ne1* also encodes protein(s) related to RuBisCO, (ii) separate and compare the RuBisCOs from the parents, ShunMai 12Ah, and ShunMai 12Af, to see if they are truly different in their SSUs and LSUs, (iii) sequence 986, 682 and 671 to reveal their AA sequences, (iv) sequence *Ne2* and *Ne1*.

Conclusion

Ne2 is a structural gene that encodes protein(s)

Based on the confirmed conclusion that *Ne2* is a dominant gene, we can also deduce that *Ne2* is a regulatory gene that encodes miRNA which targets certain protein(s). If that is the case, the presence of *Ne2* should have caused the absence of its target protein spots 986, 682 and 671, and the absence of *Ne2* should have caused the presence of its target protein spots 986, 682 and 671. The two F_{14} NIL siblings with a different composition of the *Ne2* gene, and the 2D and 2D-DIGE techs did reveal the conclusive relationship that the presence or absence of *Ne2* caused the presence or absence of protein spots 986, 682 and 671. Thus it is rational to conclude that *Ne2* is a structural gene that encodes protein(s).

The RuBisCO maladjustment model needs to be confirmed further

If further investigations on *Ne1* and/or sequencings confirm the hypothetical RuBisCO maladjustment model, it would help scientists to radically improve the photosynthetic efficiency of wheat by modifying the RuBisCO genes and/or the assembly patterns (Liu *et al.* 2010) to make more

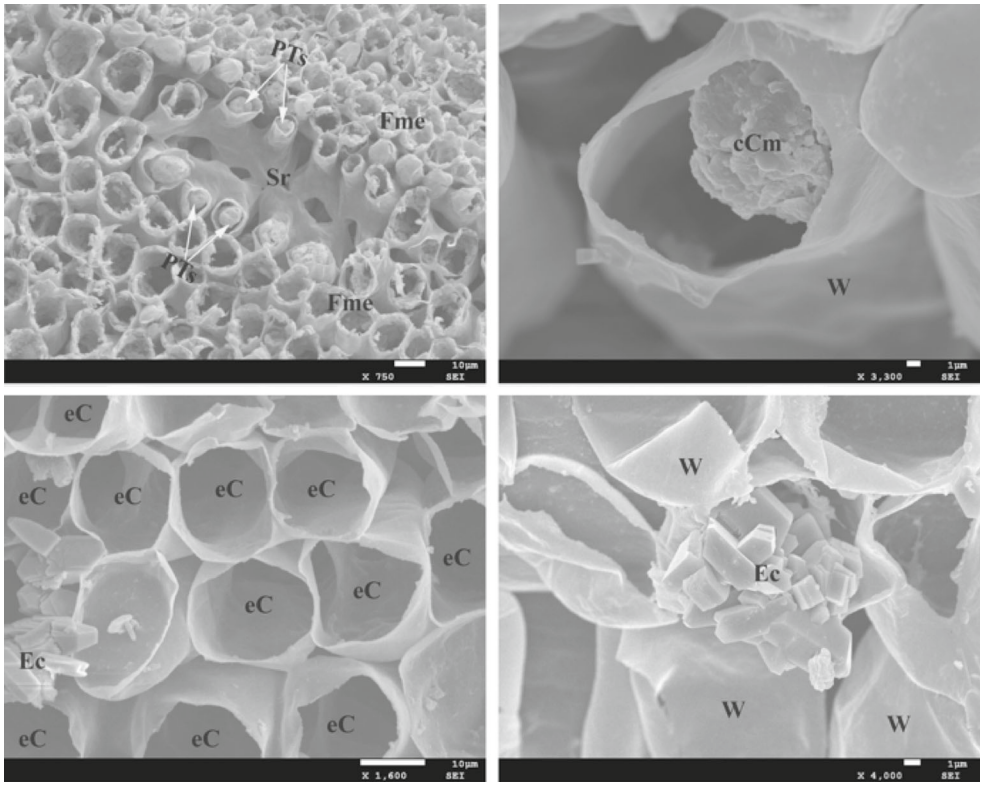

Figure 7. SEM images of the dying mesophyll cells. Fme, faveolate-mesophyll of wheat leaf blade; Sr, stoma room; PTs, plasmolysis and cytoplasm shrinkage started; cCm, condensed cytoplasmic mass; eC, empty cells with the cell wall (W) remained and unchanged; Ec, ergastic crystals (for method details see Pan *et al.* 2015b).

efficient use of light, CO_2 and water to increase sustainable global food security.

Acknowledgements

We acknowledge the National Natural Science Foundation of China (grant no. 30971786) for financial support. All the protein tests were done in the labs of Shanghai Applied Protein Technology. We thank Drs Fred Magdoff (USA), Derek Smith (UK), Ming-Bo Wang (Australia) for help in searching for the age-old references on wheat hybrid necrosis and/or polishing the manuscript. We also thank Ms Lisa Brennan, English Teaching Centre, University of Liverpool, for the careful editing.

References

Bomblies K. and Weigel D. 2007 Hybrid necrosis: autoimmunity as a potential gene-flow barrier in plant species. *Nat. Rev. Genet.* **8**, 382–393.

Caldwell R. M. and Compton L. E. 1943 Complementary lethal genes in wheat, causing a progressive lethal necrosis of seedlings. *J. Hered.* **34**, 67–70.

Chu C. G., Faris J. D., Friesen T. L. and Xu S. S. 2006 Molecular mapping of hybrid necrosis genes *Ne1* and *Ne2* in hexaploid wheat using microsatellite markers. *Theor. Appl. Genet.* **112**, 1374–1381.

Dean C. P. and Dunsmuir P. 1989 Structure, evolution and regulation of rbcS genes in higher plants. *Annu. Rev. Plant Physiol. Plant Mol. Biol.* **40**, 415–439.

Evans J. R. and Austin R. B. 1986 The specific activity of RuBisCO in relation to genotype in wheat. *Planta* **167**, 344–350.

Farisa J. D., Zhang Z. C., Lu H. J., Lua S., Reddy L., Cloutier S. *et al.* 2010 A unique wheat disease resistance-like gene governs effector-triggered susceptibility to necrotrophic pathogens. *Proc. Natl. Acad. Sci. USA* **1**, 6.

Hermsen J. G. T. 1963a Sources and distribution of the complementary genes for hybrid necrosis in wheat. *Euphytica* **12**, 147–160.

Hermsen J. G. T. 1963b The genetic basis of hybrid necrosis in wheat. *Genetica* **33**, 245–287.

Jiang Q. Y., Chen H., Pan X. L., Pan Q. Y., Shi Y. H., Li X. R. *et al.* 2008 Proteomic analysis of wheat (*Triticum aestivum* L.) hybrid necrosis. *Plant Sci* **175**, 394–401.

Kenan-Eichler M., Leshkowitz D., Tal L., Noor E., Melamed-Bessudo C., Feldman M. *et al.* 2011 Wheat hybridization and polyploidization results in deregulation of small RNAs. *Genetics* **188**, 263–272.

Khanna-Chopra R., Dalal M. G., Kumar P., Laloraya M. 1998 A genetic system involving superoxide causes F_1 necrosis in wheat (*T. aestivum* L.). *Biochemi. Biophysiol. Res. Commun.* **248**, 712–715.

Kostyuchenko I. A. 1936 The premature perishing of the hybrids in wheat crosses. *Bull. Appl. Bot. Genet. Plant Breed. Ser. V-A Wheat* **19**, 127–137 (in Russian).

Liu C., Young A. L., Windhof A. S., Bracher A., Saschenbrecker S., Rao B. V. *et al.* 2010 Coupled chaperon action in folding and assembly of hexadecameric Rubisco. *Nature* **463**, 197–202.

Mehta R. A., Fawcett T. W., Porath D. and Mattoo A. K. 1992 Oxidative stress causes rapid membrane translocation

and in vivo degradation of ribulose-1,5-bisphosphate carboxylase/oxygenase. *J. Biochem.* **267**, 2810–2816.

Naskidashvili P., Naskidashvili M., Naskidashvili I., Gakharia N. 2010 Revealing genes of hybrid necrosis and red hybrid chlorosis in crosses of varieties of georgian wheat and the importance of these genetic phenomena for selection and theoretical research. *Bull. Georgian Natl. Acad. Sci.* **4**, 145–150.

Pan X. L., Jiang Q. Y., Pan Q. Y., Wen X. F., Shi Y. H., Wang Y. J. *et al.* 2009 Proteomic analysis of hybrid necrosis in wheat (*Triticum aestivum*) leaves. *Funct. Plant Biol.* **36**, 251–259.

Pan X. L., Pan S. R., Shi Y. H., Pan Q. Y., Zhang L., Pan T. Y. *et al.* 2015a Registration of the wheat line ShunMai yyAh for hybrid necrosis. *J. Plant Register.* **9,** 407–410.

Pan X. L., Pan S. R., Zhang G. Y., Shi Y. H., Zhang L., Yao M. P. *et al.* 2015b Anatomy of wheat flag leaf blade. *Wheat Res.* **36**, 1–33 (in Chinese).

Pukhalskiy V. A., Martynov S. P. and Dobrotvorskaya T. V. 2000 Analysis of geographical and breeding-related distribution of hybrid necrosis genes in bread wheat (*Triticum aestivum* L.). *Euphytica* **114,** 233–240.

Toxlpeus H. and Hermsen J. G. T. H. 1964 Chloroplast degeneration as a consequence of "hybrid necrosis" in wheat. *Euphytica* **13**, 29–32.

Received 25 February 2016, in final revised form 12 August 2016; accepted 22 August 2016
Unedited version published online: 25 August 2016
Final version published online: 17 June 2017

Corresponding editor: ARUN JOSHI